Multi-source data assimilation of Sentinel-2 reflectance and SMAP soil moisture into APSIM for maize biomass estimation

Manuela Montella
University of Trier
Christian Bossung
Luxembourg Institute of Science and Technology
Thanh Huy Nguyen
Luxembourg Institute of Science and Technology
Marco Chini
Luxembourg Institute of Science and Technology
Jean François Iffly
Luxembourg Institute of Science and Technology
Thomas Udelhoven
University of Trier
Julia Kubanek
European Space Research and Technology Centre
Zoltan Szantoi
European Space Research Institute
Miriam Machwitz
miriam.machwitz@list.lu
Luxembourg Institute of Science and Technology

Research Article

Keywords: Crop growth modelling, Data assimilation, Particle filter, APSIM, Sentinel-2, SMAP

Posted Date: March 26th, 2026

DOI: https://doi.org/10.21203/rs.3.rs-9073727/v1

Additional Declarations: No competing interests reported.

Multi-source data assimilation of Sentinel-2 reflectance and SMAP soil moisture into APSIM for maize biomass estimation

Manuela Montella[1,2], Christian Bossung[2], Thanh Huy Nguyen[2], Marco Chini[2], Jean François Iffly[2], Thomas Udelhoven[1], Julia Kubanek[3], Zoltan Szantoi[4,5], Miriam Machwitz[2*]

[1]Department of Remote Sensing, University of Trier, 54286 Trier, Germany

[2]Remote Sensing and Ecosystems, Luxembourg Institute of Science and Technology (LIST), 'Environmental Research and Innovation' department (ERIN), Belvaux, Luxembourg

[3]European Space Research and Technology Center, European Space Agency, Noordwijk, Netherlands

[4]Directorate of Earth Observation Programmes, European Space Agency (ESA), Frascati, Italy

[5]Department of Geography and Environmental Studies, Stellenbosch University, Stellenbosch, South Africa

*corresponding author: miriam.machwitz@list.lu

Abstract

Purpose Crop growth models (CGM) are valuable tools for agricultural monitoring. However, the need for many input parameters, the uncertainties related to model parametrization and structure, and the lack of spatial information motivate the application of techniques such as data assimilation (DA). This paper proposes a DA framework to improve maize biomass estimation.

Methods A particle filter (PF) was used to assimilate remotely sensed reflectance and soil moisture (SM) data, both independently and simultaneously, into the Agricultural Production Systems sIMulator (APSIM) model. Reflectance observations from Sentinel-2 were assimilated through coupling APSIM with the radiative transfer model (RTM) PROSAIL, while SMAP L-band SM products were directly assimilated into APSIM.

Results The synthetic experiment, designed to evaluate the reliability of the proposed procedure, highlighted the strength of assimilating reflectance to constrain crop traits and of SM to reduce ensemble spread and improve robustness. Real-case results confirmed these findings. DA assimilation of SM especially contributed to improving overall biomass accuracy, particularly under data gaps and drought conditions. Although it did not consistently surpass single-source assimilation, the joint assimilation yielded consistent results. In 2022, it achieved a root-mean-square error (RMSE) of 2275.20 kg/ha, a normalized RMSE (nRMSE) of 44.99%, and a bias of 1081.90 kg/ha. In 2023, RMSE, nRMSE and bias were 1120.29 kg/ha, 14.79%, and 284.05 kg/ha, respectively. Furthermore, the joint assimilation led to a tighter ensemble spread than single source-assimilation.

Conclusion The proposed framework demonstrates the potential of multi-source DA to enhance biomass estimation and support robust, spatially explicit crop monitoring.

Keywords: Crop growth modelling · Data assimilation · Particle filter · APSIM · Sentinel-2 · SMAP

Introduction

Globally, about 680 million people suffered from food insecurity in 2024 (The State of Food Security and Nutrition in the World 2025, 2025). Agriculture determines the global food supply and is therefore directly related to food security (Gavasso-Rita et al., 2024). However, global climate change, land degradation and water scarcity have negative effects on crop production, threatening food security. Therefore, accurate crop growth monitoring is crucial for the optimization of agricultural production strategies (Yan Li et al., 2014; Luo et al., 2023; Xie et al., 2017; Zhuo et al., 2019).

Crop growth models (CGMs) can provide continuous information on the state of a crop. These models take into account different components of a system, such as soil, climatic conditions, management practices and their interactions and quantitatively simulate the entire growth process of field crops in terms of different aspects (above-ground biomass, root biomass, leaf area, etc.) (Huang et al., 2019a; Zhang et al., 2016). Since the late 1960s (Passioura, 1996), numerous CGMs have been developed and based on their main driving factors, they can be classified into four categories: soil moisture (SM), atmospheric factor, light energy, and integrated factor-driven models (Luo et al., 2023). SM-driven models highlight the interaction with SM during crop growth, and examples include AquaCrop (Steduto et al., 2009) and SWAP (van Dam et al., 2008). Atmospheric factor-driven models, such as WOFOST (van Diepen et al., 1989), focus on the influences of atmospheric O_2, CO_2, and moisture on crop growth. Light energy-driven models consider the interaction between dry matter accumulation and light energy use, with examples like LINTUL (Ezui et al., 2018) and SAFY (Ma et al., 2022). Integrated factor-driven models consist of multiple physiological sub-modules used to simulate crop growth and development while standardising inputs and outputs for broad applicability. Examples include APSIM (Keating et al., 2003), EPIC (Williams et al., 1989), and CERES (Joshi et al., 2019). Among these CGMs, according to Wang et al. (2024), the most widely used are SWAP, WOFOST, EPIC and APSIM.

However, the performance of CGMs is often limited by a high demand for input parameters, which might be affected by significant uncertainties. In addition, crop models are susceptible to uncertainties in model parametrization and structure (Dorigo et al., 2007; Huang et al., 2019a; Marin et al., 2017). Furthermore, CGMs lack spatial information, being designed as point models at the field scale (Machwitz et al., 2014).

To improve crop simulation performance, many studies have successfully applied data assimilation (DA) techniques. DA methods are designed to combine complementary information from models and measurements (field or remote sensing data) into an optimal estimate of the state variable of interest (Reichle, 2008). In general, three main DA strategies have been employed: forcing, calibration, and updating (Delécolle et al., 1992). The forcing method directly replaces the simulated values with observations. Easy to implement, it has the disadvantage of transferring the observation errors directly to the model. In addition, it requires continuous data, often at a daily step (Machwitz et al., 2014; Orlova and Linker, 2023; Wagner et al., 2020). The calibration method modifies the simulation trajectory by minimizing the differences between simulated and observed state variables (Machwitz et al., 2014; Yokoyama et al., 2024). However, this approach requires high computational time (Zhang et al., 2020) and the optimized parameter values may be unrealistic (Delécolle et al., 1992; Wagner et al., 2020). Updating methods update the states as data become available (Yokoyama et al., 2024), allowing, at the same time, parameter adjustments (Moradkhani et al., 2005). Calibrating and updating methods are preferable over forcing and are the most widely used strategies. Compared to the calibrating methods, updating methods perform well with infrequent observations and usually require less computation time. In addition, updating allows addressing uncertainties in both the simulation and the data assimilated (Orlova and Linker, 2023; Wagner et al., 2020).

The Ensemble Kalman Filter (EnKF) is one of the standard updating methods (Evensen, 2003; Ziliani et al., 2022). This method uses second-order statistics for updating the states and parameters. However, it is based on linear and Gaussian assumptions, which reduces its applicability for highly nonlinear systems (Xie et al., 2017). More sophisticated methods, able to deal with non-Gaussian distributions such as the particle filter (PF), are available thanks to progressive increases in computational resources. In contrast with EnKF, the PF can adapt to any probability density function and thus offers practical solutions for nonlinear dynamical systems (Matgen et al., 2010; Ziliani et al., 2022).

Regarding the choice of observations to assimilate into the crop model, remotely sensed (RS) data are the best candidates over field measurements, as they require less labor effort (Weinman et al., 2025c). They can provide timely and extensive information that adequately represents the evolution and variation of a crop within a field (Luo et al., 2023; Weinman et al., 2025a). Previous studies have selected leaf area index (LAI), vegetation indices, reflectance, and SM as variables for assimilation. Specifically, reflectance is a radiometric measure characterized by the spectral properties of plant elements, such as leaves, and plant conditions (Machwitz et al., 2014). Since CGMs cannot simulate this quantity, a possible approach is to couple a CGM with a radiative transfer model (RTM). This coupling consists of using a subset of the crop model states to evaluate some of the RTM parameters, simulating, as a result, reflectance. Once the simulated reflectance is obtained, this can be directly compared to the measured one during DA (Weinman et al., 2025b). Examples of RTMs include SCOPE (van der Tol et al., 2009), ACRM (Kuusk, 2001), and PROSAIL (Baret et al., 1992), with PROSAIL being one of the most widely used for crops.

Several studies have already shown the potential of assimilating reflectance in CGMs. Huang et al. (2019b) assimilated synthetic surface reflectance derived from MODIS and LANDSAT satellites into the coupled model WOFOST-PROSAIL using a four-dimensional variational DA. By minimizing the root mean square difference between simulated and measured spectral reflectance and optimizing model parameters, they improved regional winter wheat yield estimates. Weinman et al. (2025a) developed a detailed coupling formulation between the DSSAT-CROPGRO crop model and SCOPE's RTM to simulate reflectance. Based on this model setting, they applied a sensitivity-based PF to assimilate synthetic Sentinel-2 data to predict tomato growth.

Aside from reflectance, crop growth is controlled by other factors, e.g., water stress. Multi-source DA has received much attention in crop model simulations in recent years. Ines et al. (2013) developed a DA framework that incorporated remotely sensed SM and LAI data into the CERES-Maize model using the EnKF algorithm. The results suggest that assimilating LAI or SM independently slightly improved yield prediction accuracy, and that assimilating LAI and SM simultaneously considerably improved the results. Pan et al. (2019) implemented a joint LAI and SM assimilation scheme for Sentinel-1 and Sentinel-2 data in the WOFOST model to simulate winter wheat yield. They found that LAI assimilation provided better results over SM, and, because of the interaction between LAI and SM, the joint assimilation had a better performance. Zhang et al. (2022) assimilated synthetic observations of wheat and soil states into the APSIM crop model using an EnKF. While the single observations assimilation, especially of LAI and SM, improved yield estimation, their joint assimilation led to yield overcorrection. Therefore, they recommended the assimilation of only one state variable for yield prediction. SM has emerged as an effective choice for assimilation in crop models due to its relation to the atmosphere, soil and plants (Charoenhirunyingyos et al., 2011). SM is potentially useful for sequential DA, given its evident influence on crop growth.

Suitable spatial and temporal resolution data are required for a successful assimilation of RS observations into CGMs (Huang et al., 2015; Machwitz et al., 2014). The optical satellite Sentinel-2 proved to be ideal for assimilation into crop models due to its high spatial and temporal resolution (Liu et al., 2021). Unfortunately, even with the 5-day revisit time of Sentinel-2, cloud-free images are hard to obtain. Optical RS data cannot penetrate through clouds and are therefore often limited by cloud cover and rainfall, especially in regions like Central Europe (Huang et al., 2015). In such situations, microwave sensors can acquire information about the earth's surface under all weather conditions with day-night capability (Kaur et al., 2023). Serving as one of the most promising techniques to monitor surface SM, microwave RS can provide continuous and global SM data (Zhao et al., 2025; Zheng et al., 2018). Microwave sensors reported in literature include, for example, L-band based soil moisture and ocean salinity (SMOS) mission (Kerr et al., 2001), advanced microwave scanning radiometer-2 (AMSR-2) (Njoku et al., 2003), and soil moisture active and passive (SMAP) (Entekhabi et al., 2014). In this view, microwave products can fill the data gaps of optical observations, allowing for more consistent and reliable crop monitoring.

In this study, a DA framework is proposed to improve biomass estimation of maize by assimilating remotely sensed SM and reflectance into the crop model APSIM both independently and simultaneously. SM products from the L-band SMAP mission were directly assimilated into APSIM. For the assimilation of reflectance, Sentinel-2 observations were linked to APSIM via the RTM PROSAIL, with APSIM output variables used as inputs to PROSAIL. DA was realized through the application of a PF. The method was first tested via a synthetic experiment to analyze the model chain under controlled conditions. It was then applied to real data, for which independent validation information was available on two fields for two different years. Finally, a pixel-based assimilation of RS data was performed, providing biomass maps based on Sentinel-2. This approach was fundamental to moving from the region-averaged information provided by APSIM to accounting for spatial variability in biomass. Accordingly, we tested the following hypotheses: (1) joint assimilation of reflectance and SM can provide more accurate biomass estimates than single-variable assimilation. (2) SMAP data increase the robustness and temporal consistency of the DA by mitigating gaps in optical observations.

Materials and methods

Study site and field data

The data were collected during two field campaigns, which took place in the summers of 2022 and 2023 on two neighbouring fields, cultivated with maize. Both fields are located close to Everlange (49.46 ° N, 5.56 ° E) in the midwestern part of Luxembourg (Fig. 1). About half of the country is dominated by agricultural land, with half of this utilized as grassland (meadows and pasture) and half as arable land (Ministère de l'Agriculture, de l'Alimentation et de la Viticulture, 2023; Schley et al., 2008). Luxembourg has a temperate semioceanic climate with mean temperatures ranging from 0.7 °C in January to 17 °C in July. The mean annual rainfall is approximately 750 mm (Stevens et al., 2010). The soil consists of silt loam to silty clay loam textures derived from Luxembourg sandstone.

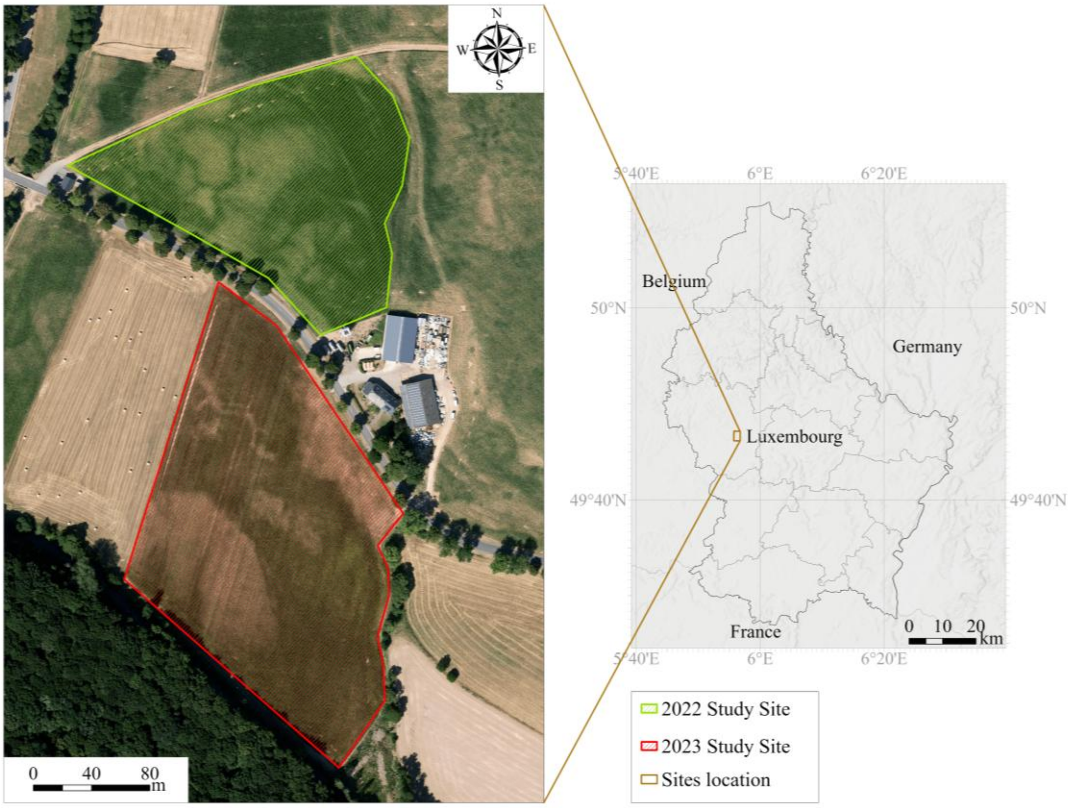

Fig. 1 – Study sites. (Source: Esri, 2015, July 7; Europe NUTS 0 Demographics and Boundaries, 2023;Luxembourg Canton Boundaries, 2025; World Imagery, 2009)

Fresh and dry biomass were collected and analyzed at four and seven dates over the growing seasons 2022 and 2023, respectively. Sowing density was calculated by measuring row spacing and the number of plants per row. 10-12 plants have been collected randomly in the field and have been dried at 105°C until a constant weight was reached. Fresh and dry biomass was calculated by the average weight per plant multiplied by the sowing density. A summary of the collected biomass is provided in Table 1. The samples collected on 12 and 21 June 2023 were excluded from the analysis because there was no DA prior to these dates. The sample collected on 26 July 2023 was also excluded because of its anomalous value. To take into account is the rather high standard deviation, which points to substantial spatial heterogeneity and increased uncertainty of the mean biomass values. Additionally, the fields have been equipped with SM sensors (Campbell CS 650 https://www. campbellsci.com/cs 650) at four locations in the field at 100 mm depth. The measurements were converted to daily values using simple averaging.

Table 1 - Measured dry biomass.

Year	Date	DOY	Dry biomass ± standard deviation (kg/ha)
2022	4 July	185	2148.9 ± 1207.85
	12 July	193	2431.65 ± 1420.29
	1 August	213	7003.5 ± 2963.84
	7 September	250	8643.45 ± 4065.48
2023	12 June*	163	38.73 ± 32.31
	21 June*	172	315.39 ± 188.66
	4 July	185	1767.87 ± 855.24
	18 July	199	5013.87 ± 2177.18
	26 July*	207	11426.15 ± 2359.62
	11 August	223	8689.96 ± 2764.42
	7 September	250	14822.18 ± 3930.04

**Discarded*

APSIM

The Agricultural Production Systems sIMulator (APSIM) Next Generation model, an updated version of the APSIM Classic model (Yanyan Li et al., 2025), is a comprehensive modelling framework designed to simulate complex and diverse agricultural systems (Holzworth et al., 2018). Details about APSIM can be found at https: //apsimnextgeneration.netlify.app/. Precipitation (daily sum), temperature (daily min/max) and solar radiation are required to drive the model. The maize model and the management modules for planting, harvesting and fertilizer were adopted. The maize model within APSIM is built using the Plant Modelling Framework (PMF) developed by Brown et al. (2014). It simulates the dynamics of crop growth, including grain yield and biomass, in response to climate and management conditions (Keating et al., 2003).

Soil input parameters for APSIM were downloaded from the SoilGrid dataset, which provides global estimates of key soil properties, such as organic carbon, pH, bulk density, soil texture fractions, cation exchange capacity (CEC), and coarse fragments, at seven standardized depths (0, 50, 150, 300, 600, 1000, and 2000 mm) (Hengl et al., 2017). Weather data, including temperature, precipitation, and solar radiation, were collected during the growing season by a weather station installed in the field. To model an entire year, these data were extended by a weather station maintained by the Administration of Technical Agricultural Services Luxembourg (ASTA) at about 2.5km from the study site (ASTA, 2026). During the growth season of maize, the daily mean temperature was 16.8 °C, and the total precipitation ranged from 257 to 307 mm during 2022-2023 (Table 6). The farmer provided information about the management practices for both years. For both fields, the previous crop was mustard, planted on 21 October 2021 and 5 October 2022, respectively. Maize was sown at a depth of 50 mm on 3 May 2022 and on 7 May 2023, and harvested on 13 September 2022 and 11 September 2023, respectively. Before sowing maize, fertilizer was applied at a rate of 200 kg/ha using Potassium Ammonium Sulfate and 40 m^3/ha using sludge, on 1 May 2022 and 6 May 2023, respectively, in both fields. Since information about the maize cultivars for both fields was not available, the German maize variety "Companero", calibrated and tested in APSIM for temperate European zones by Knörzer et al. (2011), was adopted.

PROSAIL

In order to assimilate satellite reflectance data into the APSIM model, the RTM PROSAIL-D (V5) was applied in forward mode to generate reflectance values. For the parametrization of PROSAIL, outputs from APSIM were used. PROSAIL integrates the leaf optical properties model PROSPECT (Jacquemoud et al., 2009) with the SAIL model (Verhoef, 1984), which simulates radiative transfer through a turbid vegetation canopy. The two models are linked by using the leaf reflectance and transmittance outputs from PROSPECT as inputs to SAIL, along with data on soil optical properties and the illumination and observation geometry (Berger et al., 2018).

The list of PROSAIL input parameters is provided in Table 2. As shown in Fig. 2, the LAI was directly transferred from APSIM to PROSAIL, while the remaining PROSAIL input parameters (marked in grey) were computed from APSIM outputs. The leaf angle distribution function (LIDFa) was assigned according to the phenological growing stage of the maize crop simulated by APSIM, as described by Su et al. (2019) (see Table 7 in Appendix).

Data assimilation framework

DA techniques assume that the observation is related to the true state x_t (e.g., biomass at time t) by:

$$y_t = H(x_t) + v_t \tag{1}$$

where y_t is the observation, $H(\cdot)$ is the observation operator that translates the state variables to the observation, and v_t represents the observation error.

The temporal evolution of the crop model state variables is described by:

$$x_t = M(x_{t-1}, u_t, b) + q_t \tag{2}$$

where $M(\cdot)$ is the nonlinear model operator, u_t represents external inputs such as weather or management data, b denotes model parameters, and q_t accounts for model errors.

Within the Bayesian framework, both prior knowledge and observations are represented by probability density functions (PDFs). As new observations become available, the prior PDF is updated to form the posterior distribution of the state variables. Due to the complexity and nonlinearity of crop models, obtaining an analytical expression for this posterior is generally infeasible. To overcome this limitation, PFs are particularly advantageous, as they approximate the posterior PDF using a finite ensemble of weighted particles (Huang et al., 2024a). Unlike Kalman filters, which are widely used, PF does not restrict the observation and the probability distribution of the prior sample as Gaussian, thus allowing its use for nonlinear, non-Gaussian dynamic systems (Jiang et al., 2014).

The PF is a sequential Monte Carlo method that combines sequential importance sampling (SIS) and resampling (Douc et al., 2005). In SIS, particles $x_t^{(i)}$ are sampled from a proposal distribution and assigned importance weights $w_t^{(i)}$. When a new observation y_t becomes available, the likelihood of each particle's predicted observation $Hx_t^{(i)}$ is evaluated. For Gaussian observation noise, the weight of each particle is:

$$w_t^i = \frac{1}{\sigma_t\sqrt{2\pi}} \exp\left[-\frac{(y_t - Hx_t^i)^2}{2\sigma_t^2}\right] \tag{3}$$

with σ_t the standard deviation of the measurement at time t.

The weights are then normalized to sum to one, and the state estimate at time t is obtained as the weighted mean:

$$\hat{x}_t = \sum_{i=1}^{N_p} w_t^i x_t^i. \tag{4}$$

with N_p the number of particles.

A common problem in SIS is the so-called "particle degeneracy", which leads to very few particles retaining significant weights. As such, the PF becomes inefficient after having lost its variability. To avoid this, a resampling algorithm is applied. While keeping the total number of particles unchanged, this algorithm multiplies samples with high importance weights and eliminates samples with low weights (Salamon and Feyen, 2009). In this study, residual resampling was employed because of its lower variance and computational cost compared with other resampling methods.

However, resampling can lead to sample impoverishment, reducing ensemble diversity. To counter this, particles are perturbed by adding Gaussian noise following Jiang et al. (2014) and Orlova and Linker (2023):

$$\alpha_{t,pe}^i = \alpha_{t,res}^i + \eta_t^i \tag{5}$$

with

$$\eta_t^i \sim N\left(0, \left(\varepsilon_{pe}\, \alpha_{t,res}^i\right)^2\right) \tag{6}$$

where $\alpha_{t,pe}^i$ and $\alpha_{t,res}^i$ are the perturbed and resampled parameter values, η_t^i is the added noise and ε_{pe} is the tuning factor which must be specified.

Fig. 2 shows the overall framework of the PF assimilation scheme. After running the crop model APSIM with all the necessary input data, such as meteorological, crop, soil and management data, the initial particle ensemble was created. One APSIM simulation represents one particle or ensemble member. The differences among the particles arise from the perturbation of several APSIM parameters, which were selected based on their impact on the biomass results. Table 3 displays an overview of the selected parameters, their plausible ranges of variation and the number of variation steps. The perturbed parameters referred to management strategies, such as the date of sowing and plant population, to daily weather supplied to the simulation and to one of the phenological phases of the maize crop. All other management factors remained constant while perturbing the selected parameters, generating an ensemble of 66150 particles. Then, three different assimilation strategies were tested: (1)

assimilation of reflectance only (DA_R); (2) assimilation of SM only (DA_{SM}); (3) assimilation of reflectance and SM (DA_{R+SM}).

Regarding DA_R, since the observed spectral reflectance cannot be directly assimilated into a crop model, the spectral reflectance for each APSIM particle is computed by coupling APSIM with PROSAIL. Once the ensemble of spectra has been generated, a weight is assigned to each particle and each spectral band whenever a Sentinel-2 observation is available, according to Eq. (3). Here, y_t and σ_t representing the mean reflectance and its standard deviation within one crop field, while Hx_t^i denotes the simulated reflectance. The weights are then normalized and averaged across all bands, and finally normalized across all particles. In contrast, since SM is an output of APSIM, the observed SM can be assimilated directly, and weights are computed following the same approach, with y_t representing the SM value within a crop field, σ_t its standard deviation, and Hx_t^i the simulated SM. Afterwards, weights are normalized across all particles.

Once the particle weights had been calculated (either by assimilating reflectance, SM, or both), the ensemble weighted average of biomass was calculated according to Eq. (4). To compute the weighted mean of the biomass in the case of DA_R, the weights assigned to the spectra are applied backwards to the corresponding APSIM particles from which they derive.

Before performing the next DA step at the next available observation date, particles were resampled and perturbed, according to Eq. (5). This means that only the particles, and hence the parameters, with the highest weights were kept, perturbed and used to update APSIM. Particles with low weights are removed from the ensemble. Following Orlova and Linker (2023) and Weinman et al. (2025a), the tuning factor ε_{pe} in Eq. (5) was set equal to 0.08 for DA_R and to 0.02 for DA_{SM}.

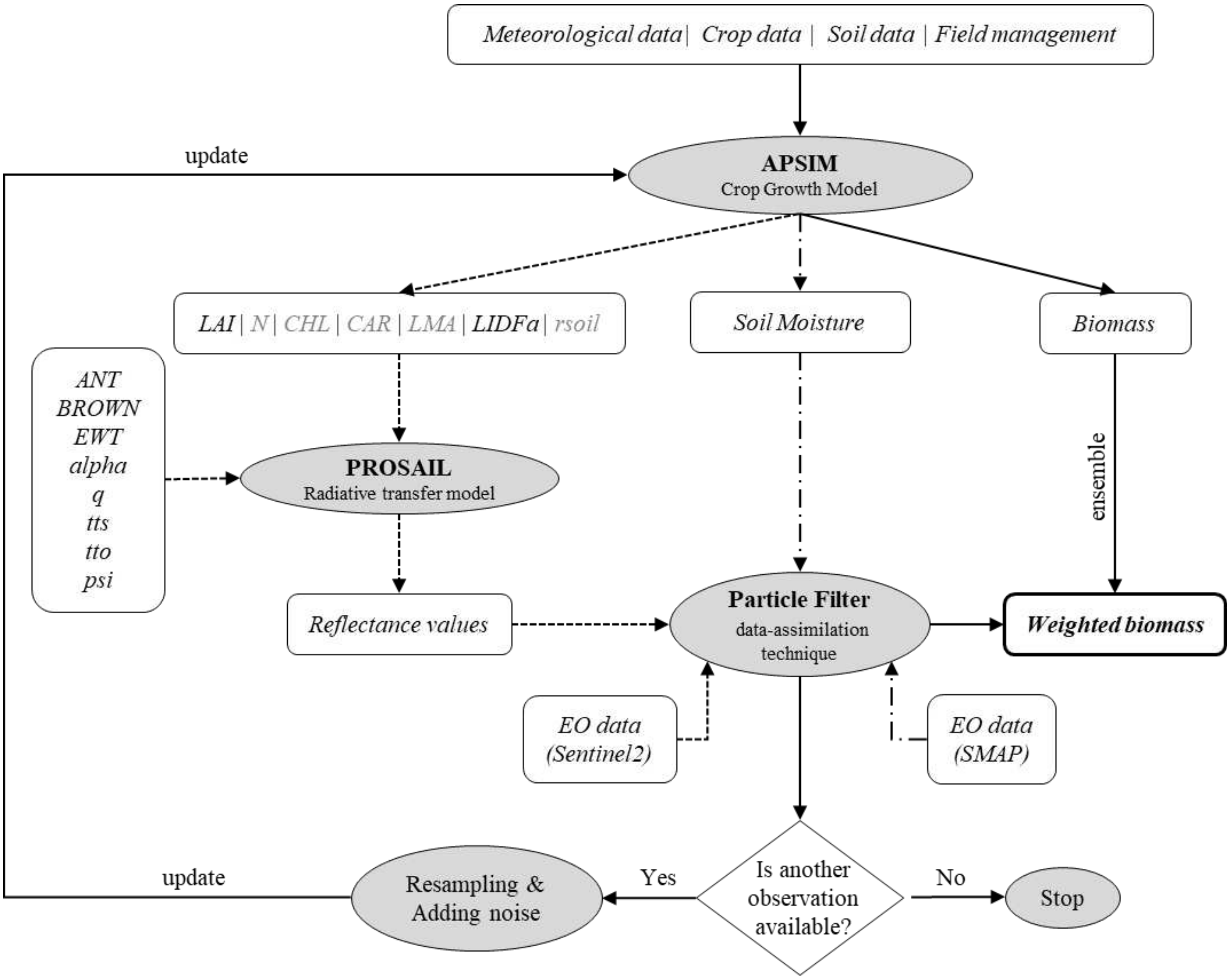

Fig. 2 - Scheme of the data assimilation-crop modelling framework with assimilation of Sentinel-2 and/or SMAP data (please refer to Table 2 for details in symbols)

Synthetic and real-case experiments

The proposed framework was first evaluated through a synthetic experiment and then applied to real data. The purpose of this synthetic experiment was to evaluate the performance of the proposed DA method (Di Mauro et al., 2021) under fully controlled settings. In this context, the "true" state was generated by a single model run, while the assimilated observations were generated by the same model run with the addition of prescribed noise. In this way, uncertainties associated with observation noise and model-data structural inconsistencies are minimized. Therefore, non-satisfactory results from the DA are due either to a fault in the modelling chain itself or to the prescribed uncertainty in the observations (Machwitz et al., 2014).

The exact initial settings (weather, soil, crop, and management conditions) were used in both experiments. The main differences between synthetic and real-case experiments lie in the assimilated measurements and validation data. For DA_R, Sentinel-2 observations were assimilated in the real-case experiments (see sub-section Remote sensing data), whereas the synthetic experiments assimilated reflectance generated by the coupled crop-radiative-transfer model. The synthetic reflectance was adjusted to match the spectral characteristics of the Sentinel-2 sensor, and the assimilation times were set to the dates when Sentinel-2 images were available during the 2022 and 2023 seasons. Following Machwitz et al. (2014), the assimilation window was set from June to August, since observations from the first half of the growing period were found to be more valuable than late-season data. For DA_{SM}, SMAP SM products were assimilated into the real-case experiments, and the APSIM simulated SM in the synthetic experiments. This synthetic SM was generated alongside the "true" biomass and served as synthetic observations, and their assimilation times were set to the dates when SMAP products were available. According to Lu et al. (2021), SM still improves biomass estimation when considering a longer assimilation interval. Therefore, SM was assimilated at 7-day intervals from June to September, where possible. Additionally, in 2023, for DA_{R+SM}, to keep a weekly assimilation frequency, when a Sentinel-2 observation was available during a given week, the corresponding SMAP observation was not assimilated for that week.

Regarding the validation data, the synthetic experiments used synthetic biomass as "true" biomass, generated by running the model with realistic settings, whereas the real-case experiments used field measurements (Table 1).

Remote sensing data

Remotely sensed data in this study consists of Sentinel-2 and SMAP products. Sentinel-2 is a European wide-swath, high-resolution, multispectral imaging mission. Characterized by three polar-orbiting satellites, Sentinel-2A, 2B, and 2C, with 2C soon replacing 2A, it delivers images over the same area every 5 days or less. It presents 13 spectral bands covering a spectrum range from 442 nm to 2100 nm, with spatial resolutions of 10, 20, and 60 m (Copernicus Data Space Ecosystem, 2023). Cloud-free Sentinel-2 imagery was downloaded from the LSA Data Center (www.collgs.lu) at Level 2A (atmospherically corrected Surface Reflectance), processed with the SeNtinel Applications Platform (SNAP) to 10 m geometric resolution and finally subset to the region of interest. Table 8 in the Appendix summarizes the Sentinel-2 bands used in this study.

In 2022, only 2 dates with images of sufficient quality were available on 31 July (DOY= 212) and 10 August (DOY= 222), while in 2023, there were 4 on 26 June (DOY= 177), on 6 July (DOY= 187), on 11 July (DOY= 192), and 10 August (DOY= 222). Following the procedure of Machwitz et al. (2014), the reflectance values were averaged over a selected area within each field and used as the observed spectrum. A standard deviation equal to 0.015 was assumed as the standard uncertainty level in the synthetic experiments for both years, whereas for the real-case experiments, the standard deviation computed for all the Sentinel-2-derived reflectance values was used.

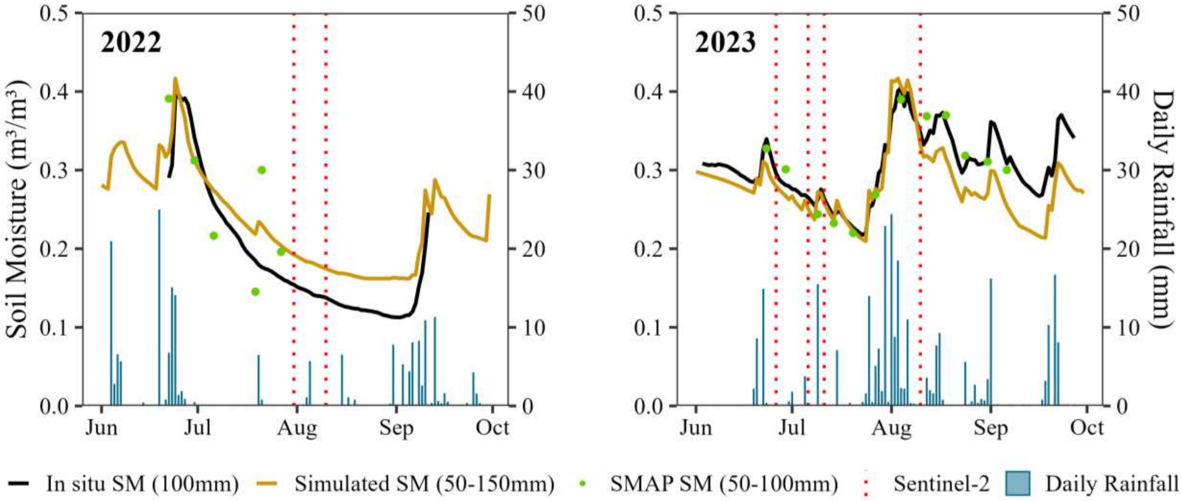

Fig. 3 - Daily in situ, satellite (SMAP) and simulated SM estimates along with rainfall and Sentinel-2 observations for the years 2022 (left) and 2023 (right).

In this work, we utilize the VanderSat/Planet volumetric Soil Water Content (SWC) L-band products at 100 m spatial resolution. They were provided by the ASTA within the Soil Humidity in Luxembourg 2002-2023 dataset. Such a product, with a temporal resolution up to 230 observations per year for Luxembourg, is derived from AMSR2 and SMAP passive microwave brightness temperatures, in combination with multispectral observations from Sentinel-2. First, the satellite observations were combined and downscaled to a spatial resolution of 1 km with the VanderSat patented technology (US10643098, EP3469516B1). The downscaled microwave observations are then converted to soil water content using the physical-based Land Parameter Retrieval Model (VUA-NASA), which solves the radiative transfer equation at different frequencies and polarizations to retrieve soil water content (Owe et al., 2008; Owe and van de Griend, 1998; van der Schalie et al., 2021). Then, to produce the SWC 100 m product, the 1 km product integrates the near-infrared and shortwave infrared bands from Sentinel-2, namely band 8 (842 nm) and band 11 (1610 nm), to introduce finer spatial constraints in the disaggregation process, resulting in enhanced spatial precision for SM estimation. This method also leverages Copernicus DEM (GLO-90), SoilGrid soil map, and land cover maps from the Copernicus Land Monitoring Service including the Global Surface Water Bodies product from PROBA-V. The overpass time of SMAP is 06:00 AM, and the sensing depth is approximately 5 cm, and can be up to 10 cm depending on the moisture condition (i.e. the drier the soil, the deeper the sensing depth) (Owe and van de Griend, 1998). The SMAP-derived estimates of SM in the top 5 cm of soil should have an error smaller than 0.04 m^3/m^3 volumetric (Entekhabi et al., 2014). It is worth noting that several data gaps exist in this dataset, including 19 June 2019 to 24 July 2019, 5 August 2022 to 24 September 2022, and 16 November 2022 to 18 November 2022.

To fully exploit the information contained in SMAP data (Reichle and Koster, 2004), a Cumulative Density Function-matching approach was employed, similar to the work of Mishra et al. (2017). This technique aims to correct satellite-based SM biases by removing systematic differences between in situ measurements and SMAP SM. For a more detailed description of this method, the reader is referred to Brocca et al. (2011). The process was applied to the SMAP products for both years and subsequently used in the assimilation scheme, as part of the observation operator H. In 2022, the SMAP SM product was available only from the end of June to the end of July (due to the gap in the data between 5 August and 24 September), whereas in 2023, the entire summer season was covered.

The daily time series of SM from SMAP, in situ observations, and APSIM are plotted along with daily rainfall and the available Sentinel-2 images for both years (Fig. 3). Overall, SMAP and the simulated SM follow closely with precipitation events. Only in late July 2022 does the SMAP product show a fluctuation not captured by the in-situ measurements and only slightly reproduced by the simulated one. To account for uncertainty in the algorithm retrieval and instrument noise, the value 0.04 $m^3\ m^{-3}$ was assumed as observation-error standard deviation (Jackson et al., 2016) in both synthetic and real experiments.

Table 2- PROSAIL input parameters with the corresponding symbols, units, formula using APSIM outputs/ fixed values and references.

Parameter	Symbol	Unit	Formula/Value	References
Leaf structure	N	-	$\frac{(0.025 + 0.9 * sla)}{(sla - 0.1)}$	(Jacquemoud et al., 2009)
Chlorophyll content	CHL	$\frac{\mu}{cm^2}$	0.0203 * $SPAD^2$ - 0.0146 * SPAD + 9.7799 with SPAD: -28.8 + 58.0*NP - 9.55 * NP^2	(Dwyer et al., 1995; Markwell et al., 1995)
Carotenoid content	CAR	$\frac{\mu}{cm^2}$	CHL / 4.11	(Feret et al., 2008)
Anthocyain content	ANT	$\frac{\mu}{cm^2}$	0	(Féret et al., 2017)
Brown pigment content	BROWN	-	0.1	(Machwitz et al., 2014)
Equivalent Water Thickness	EWT	$\frac{g}{cm^2}$	0.02	(Machwitz et al., 2014)
Leaf Mass per Area	LMA	$\frac{g}{cm^2}$	$dms/_{lai}$	(Machwitz et al., 2014)
Solid angle for incident light	alpha	-	40	(Machwitz et al., 2014)
Leaf angle distribution function	LIDFa	°	According to PhenoStage (Table 7)	(Su et al., 2019)
Leaf Area Index	lai	$\frac{m^2}{m^2}$	APSIM output	-
Hot Spot parameter	q	-	2	(Machwitz et al., 2014)
Sun zenith angle	tts	°	extracted from Sentinel-2 metadata	-
Observer zenith angle	tto	°	extracted from Sentinel-2 metadata	-
Azimuth Sun/ Observer	psi	°	extracted from Sentinel-2 metadata	-
Soil reflectance	rsoil	-	1 - (*sw* / *sat*)	(Machwitz et al., 2014)

** *sla*: specific leaf area per dry weight [$\frac{cm^2}{mg}$]; *sw*: soil water [$\frac{mm^3}{mm^3}$] of the first soil layer ; *sat*: soil water at saturation [$\frac{mm^3}{mm^3}$] of the first soil layer; *dms:* dry matter [$\frac{g}{m^2}$]; *NP:* percentage of green leaf nitrogen [%].

Result evaluation

The outcomes of the DA experiments were evaluated with the root mean square error (RMSE), the normalized RMSE (nRMSE) and the bias, expressed as:

$$RMSE = \sqrt{\frac{\sum_{1=1}^{n}(S_i - O_i)^2}{n}} \quad (7)$$

$$nRMSE = \frac{RMSE}{\bar{O}} * 100\% \quad (8)$$

$$bias = \frac{1}{n}\sum_{1=1}^{n}(S_i - O_i) \quad (9)$$

where n is the number of observations available, O and S are the observed and the simulated data, respectively, whereas $\bar{O}$ is the mean of observations, σ_O and σ_S are the standard deviations of observations and model simulations, respectively.

Each of these metrics provides information on the goodness of fit. RMSE and nRMSE illustrate the absolute and relative magnitude of the difference between simulation and observation, and the bias refers to the tendency of the simulation to over- or underestimate the observation.

Table 3 - APSIM perturbed variables, their units, range of variation, and number of variation steps.

Variable	Unit	Minimum	Maximum	step
MinT	°C	-3	+3	1
MaxT	°C	-3	+3	1
Rainfall	mm	-30%	-10%	10
Radiation	MJ/m^2	-20	+20	10
Sowing day	DOY	121	145	6
Plant population	/ m^2	5	10	1
Juvenile phase	deg day	150	250	50

Spatial biomass

Once the three strategies were tested and evaluated, a final DA_{R+SM} was performed, integrating spatial information in the modelling chain. SMAP data were assimilated to resample particles with the strongest influence, while Sentinel-2 data were assimilated on a pixel basis. For this task, a mask was applied to the Sentinel-2 images to focus on the field area, and, according to each pixel's reflectance, a different set of weights was assigned to the particles of the ensemble of APSIM biomass.

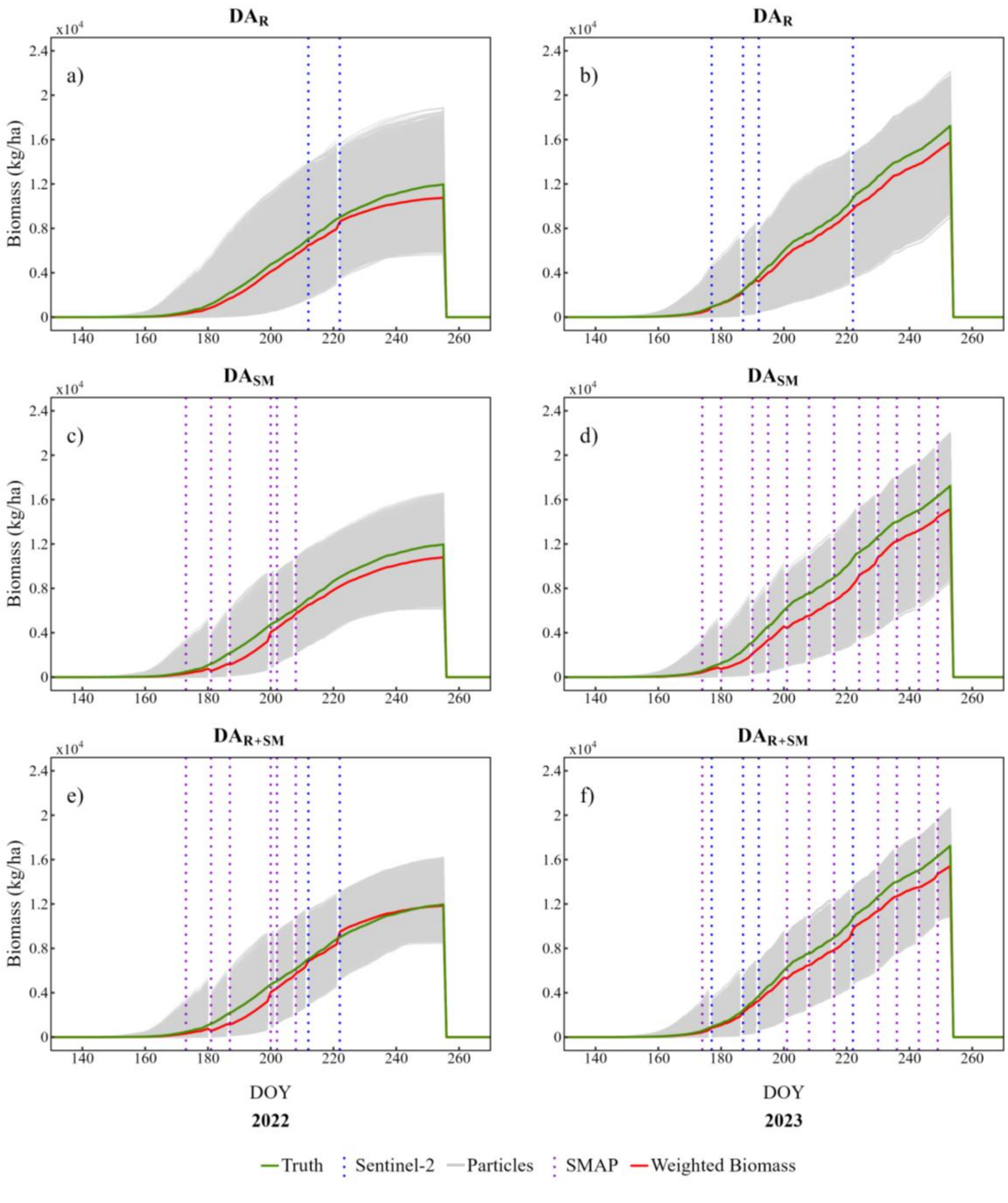

Fig. 4 - Biomass estimates from the three DA strategies for the synthetic experiment. The gray lines represent the particle ensemble.

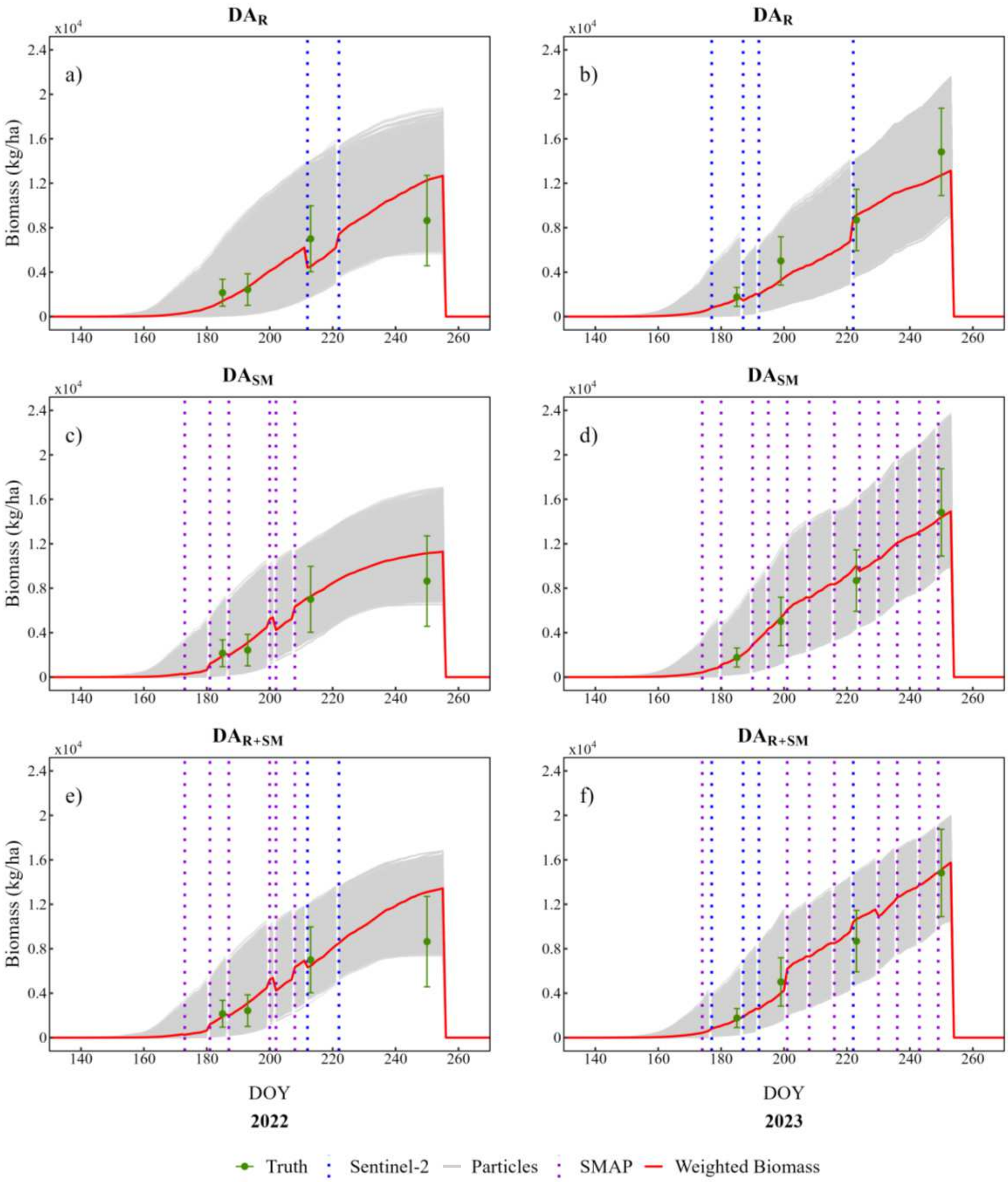

Fig. 5 - Biomass estimates from the three DA strategies for the real-case experiment. The gray lines represent the particle ensemble, the green circles are the field average measurements, and the error bars indicate the variation range of the samplings.

Results

Synthetic experiment

The variation in the APSIM input parameters, using the ranges listed in Table 3, produced an ensemble of 66150 particles for both fields, with aboveground biomass as the main simulated output. Fig. 4 displays the results of the three DA strategies for both years, and Table 4 summarizes the statistical metrics. These metrics were computed for the dates for which biomass measurements were available (see Table 1).

In 2022, two cloud-free Sentinel-2 observations were available (blue dotted lines in Fig. 4a). While the first assimilation (DOY = 212) showed no improvement, the second assimilation step (DOY = 222) shifted the biomass estimate closer to the "true" biomass. However, after a few days, the weighted biomass decreased slightly. Regarding DA_{SM}, no SMAP data were available after August (see section Remote sensing data), while many dates were missing in July, resulting in a total of six assimilation steps (violet dotted lines in Fig. 4c). Early assimilation (DOY = 181, 187) caused biomass underestimation. From the fourth assimilation onwards (DOY = 200), the weighted biomass was dragged closer to the "true" one. DA_{R+SM} (Fig. 4e) showed a similar pattern to DA_{SM}. However, the assimilation of simulated reflectance (DOY = 212, 222) produced a clear improvement, with biomass estimates closer to the synthetic truth.

In 2023, four cloud-free Sentinel-2 observations were available (Fig. 4b). The first two assimilations (DOY=177, 187) updated the weighted biomass close to the "true" biomass. A slight downward drift occurred after the third assimilation (DOY=192), and this state was maintained through the final update (DOY=222). SMAP data were available for the entire season, allowing assimilation once per week (Fig. 4d). Improvements from DA_{SM}were limited, with persistent biomass underestimation except for a brief improvement in late August. DA_{R+SM} performed similarly to DA_R, with the assimilation of reflectance correcting the SM-driven underestimation.

In both seasons, DA_R yielded the best results in terms of RMSE and nRMSE (2022: RMSE =737.51 kg/ha, nRMSE = 12.27%; 2023: RMSE = 917.41 kg/ha, nRMSE = 10.39%). In 2022, DA_{R+SM} achieved the lowest bias (-569.48 kg/ha), while in 2023, the bias (-895.62 kg/ha) was slightly higher than for DA_R (-798.16 kg/ha). For both years, DA_{R+SM} produced a markedly smaller ensemble size than the other strategies, indicating a tighter resampling of parameter sets.

Table 4 – Goodness of fit metrics for biomass estimates for the two growing seasons under different simulation strategies in the case of the synthetic experiment.

Year	Experiment	Strategy	RMSE	nRMSE	Bias
2022	Synthetic	DA_R	737.51	12.27	-689.00
		DA_{SM}	976.16	16.24	-939.53
		DA_{R+SM}	746.36	12.42	-569.48
2023	Synthetic	DA_R	917.41	10.39	-798.16
		DA_{SM}	1741.15	19.71	-1632.85
		DA_{R+SM}	1027.893	11.64	-895.62

Assimilation of Sentinel-2 and SMAP real data

In the real case study, Sentinel-2 reflectance and SMAP SM were assimilated. For each Sentinel-2 acquisition, band-specific means and standard deviations were extracted for each field. SMAP SM data were extracted from the pixels covering both fields, and the uncertainty was set to a literature-based value. Weighted biomass estimates were evaluated against field measurements collected on four dates in 2022 and in 2023 (Table 1). Results for the three DA strategies are shown in Fig. 5, and the metrics are reported in Table 5.

In 2022, DA_R (Fig. 5a) behaved similarly to the synthetic experiment. The first assimilation did not improve biomass estimates and shifted the weighted state downward, remaining within the observed biomass range but underestimating its mean. The second assimilation corrected this bias, but in the absence of further updates, the propagated state produced an overestimation later in the season. Better results were obtained with DA_{SM} (Fig. 5c), which closely fit the observation. However, the absence of SMAP data after July prevented further correction in the late season. DA_{R+SM} (Fig. 5e) provided only a limited improvement over DA_R, although the inclusion of SM partially mitigated the deviations introduced by reflectance-only assimilation.

In 2023, DA_R (Fig. 5b) improved compared with 2022. The second and third assimilation steps led to an underestimation of biomass, which was then corrected by the final assimilation. Overall, DA_R maintained estimates within the observed biomass range. DA_{SM} delivered the best results (Fig. 5d), where the final assimilation resulted in close biomass estimation compared to the last observation. When combined with reflectance (Fig. 5f), SM helped to correct for the mid-season underestimation in DA_R, resulting in a good fit at the end of the season. DA_{R+SM} also produced a reduced ensemble size, consistent with the synthetic experiment.

Overall, DA_{SM} performed best in the real-case experiments, particularly in 2023 (RMSE = 728.68 kg/ha, nRMSE = 9.62%). In 2022, DA_{R+SM} showed the poorest performance (RMSE = 2275.2 kg/ha, nRMSE = 44.99%) and a significant positive bias (~1082 kg/ha). In 2023, by contrast, it achieved the lowest bias (~284 kg/ha) and outperformed DA_R (RMSE = -888.72 kg/ha, nRMSE = 18.22%).

Table 5 - Goodness of fit metrics for biomass estimates for the two growing seasons under different simulation strategies in the case of the real-case experiment.

Year	Experiment	Strategy	RMSE	nRMSE	Bias
2022	Real	DA_R	2232.62	44.15	145.97
		DA_{SM}	1305.16	25.81	788.42
		DA_{R+SM}	2275.20	44.99	1081.90
2023	Real	DA_R	1379.69	18.22	-888.72
		DA_{SM}	728.68	9.62	310.03
		DA_{R+SM}	1120.29	14.79	284.05

Fig. 6 shows the results of the modelled biomass after applying the PF on a pixel basis for both years. The displayed biomass ranges between 700 and 10,500 kg/ha, covering the temporal evolution of biomass for both fields. In 2022, the resulting maps (Fig. 6 a), b)) showed limited spatial variability across the field, with the spatial range of the estimated biomass remaining low (~40 kg/ha). In contrast, in 2023 parts with high and low productivity can be clearly distinguished, with pronounced spatial patterns already evident at early- (Fig. 6 c), d)) and mid-season stages (Fig. 6 e), f)). Due to a lack of samples distributed over the entire field, a spatially explicit evaluation was not possible.

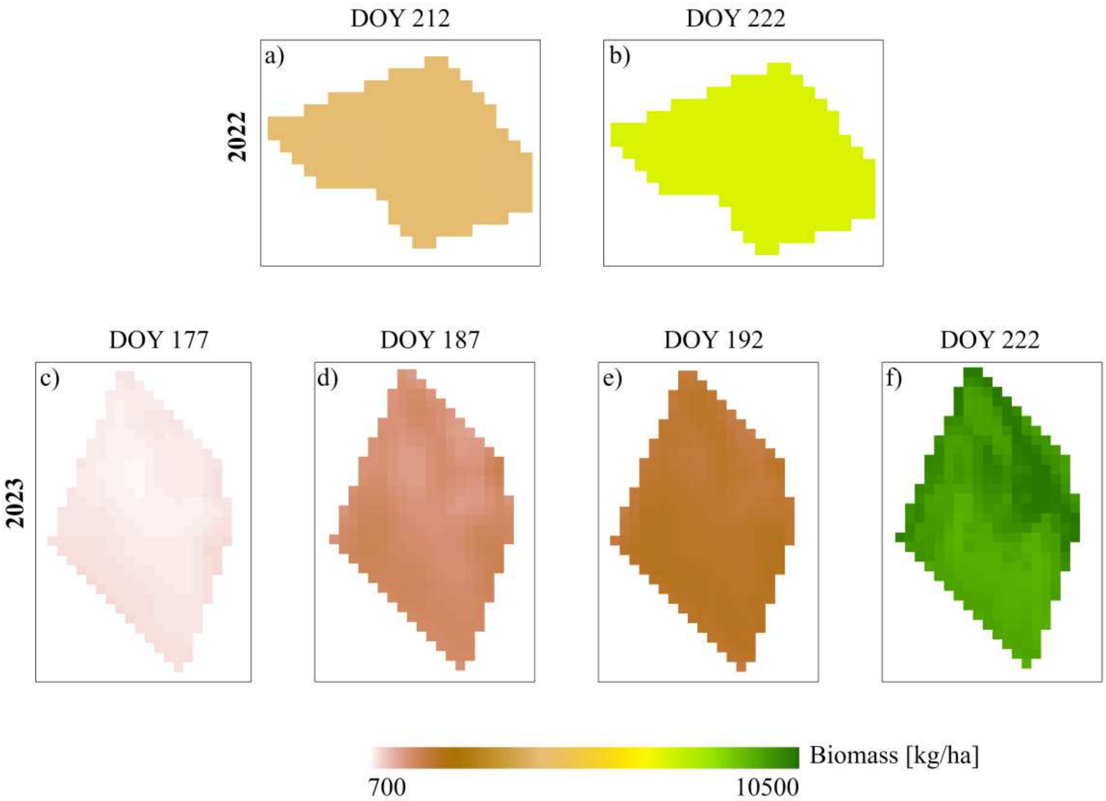

Fig. 6 - Biomass estimation for maize in 2022 (top) and 2023 (bottom) based on the DA_{R+SM}.

Discussion

In this study, a DA scheme was developed to improve biomass estimation by assimilating reflectance and SM into the crop model APSIM, both independently and simultaneously. The PF ensemble was generated by perturbing APSIM input parameters. Through the DA scheme, parameters more consistent with the observations were resampled and propagated. Consequently, the effectiveness of each assimilation strategy strongly depended on the link between observations, model states and perturbed parameters.

Under synthetic conditions, where structural and observational uncertainties were minimized, DA_R provided the best performance, followed closely by DA_{R+SM}, while DA_{SM} showed a slight decrease in accuracy. Reflectance can provide timely information on the substantial and gradual changes in several biochemical and biophysical plant characteristics, measurable within distinct spectral ranges (Hendawy et al., 2019; Lobos et al., 2019). In contrast, a change in SM availability in the soil does not immediately affect biomass, but influences crop growth indirectly through plant water stress, with a time lag of days or weeks (Li et al., 2022). As a result, SM assimilation alone exerted a weaker direct influence on biomass estimation. Our results are consistent with a previous study based on synthetic SM assimilation. El Sharif et al. (2015) assimilated SMAP-type SM data into the DSSAT-CSM and showed that mean crop yield was not significantly improved, whereas the uncertainty of simulated yield was reduced by up to 30%. In our case, a similar mechanism was observed. SM assimilation showed only a modest impact on biomass estimation. However, it improved ensemble constraints by filtering out improbable simulations, reducing ensemble spread and tightening parameter-set resampling. This behavior was also observed in the joint assimilation, where the ensemble spread was reduced even further, whereas the inclusion of reflectance improved biomass estimation by directly constraining vegetation states. These results suggest that, under ideal conditions, SM contributes mainly to robustness and temporal consistency rather than to the improvement of accuracy.

In the real-case experiment, Sentinel-2 and SMAP data were assimilated. For both 2022 and 2023, DA_{SM} achieved the lowest RMSE and nRMSE, showing its positive effect on the DA scheme. Especially in 2023, assimilating SM together with reflectance reduced the error compared with DA_R and also produced the smallest bias. This positive effect was less pronounced in 2022, where DA_{R+SM} showed lower accuracy compared to the other strategies. Moreover, the assimilation of real SM led to a smaller ensemble spread, particularly in 2022. This reduction of the ensemble spread became more pronounced in the joint assimilation, as already seen for the synthetic experiments.

Less effective was the performance of DA_R, specifically in 2022. The assimilation of reflectance led to higher error in 2022 than in 2023, and the reasons might be attributed to the following: (1) only two observations were available in 2022, both acquired at a late growth stage of maize. The time window of data acquisition has a significant impact on DA efficiency (Machwitz et al., 2014; Weinman et al., 2025a; Zhang et al., 2022), and the limited window assimilation in 2022 was probably insufficient to capture key development processes of maize. In contrast, the more observations available in 2023 were also covering earlier stages of the growing season, allowing the system to better capture crop dynamics. (2) The year 2022 was affected by a severe drought. Previous studies have shown that, under dry conditions, the assimilation of LAI or canopy cover can increase plant water stress, thereby reducing the accuracy of yield estimates (Ines et al., 2013; Liu et al., 2021; Lu et al., 2021; Zhang et al., 2020).

When comparing the results of DA_R between the real-case and synthetic experiments, better performance is observed in the synthetic experiment. When assimilating real reflectance data, in addition to the uncertainties associated with the Sentinel-2 instrument (e.g. atmospheric correction errors, mixed pixels, etc.), there are the uncertainties arising from the coupling of APSIM with PROSAIL (Machwitz et al., 2014; Weinman et al., 2025c), which were not accounted for and may therefore have, to some extent, influenced the DA process.

In our framework, assimilating real SM data substantially improved biomass estimation relative to reflectance-only assimilation, reducing RMSE by 42% (~930 kg/ha) in 2022 and 47% (~651 kg/ha) in 2023. The strong contribution of SM can be attributed to lower uncertainties injected in the system. Since the simulated SM is a direct output of APSIM, its assimilation avoids uncertainties associated with the PROSAIL coupling. In addition, there is a direct physical link between SM and crop water stress, which strongly controls growth processes in APSIM.

Other studies confirm the significant impact of SM assimilation on estimation results, especially for water limited conditions. Zhuo et al. (2019) reduced the error in prediction by about 396 kg/ha for wheat modelling in Hengshui city, China, by assimilating SM retrieved from Sentinel-1 C-band SAR and Sentinel-2 MSI optical data. Using a multistep assimilation framework, Zhang et al. (2020) found that SM assimilation contributed to improving yield estimation of wheat, reducing the RMSE by 47% compared with LAI and crop phenology assimilations in the North China Plain. In a study by Chakrabarti et al. (2014), downscaled SM derived from the SMOS mission was assimilated, and the yield of soybean in La-Plata Basin, Brazil, was estimated. Results showed a considerable improvement in yield, with differences between the assimilated and observed crop yields of 16.8% and 4.37% during the wet and dry growing seasons, respectively. In our case, the accuracy of biomass was lower in 2022, the year affected by drought, probably because there were no available data in August and September to update and correct biomass as in the previous months.

The DA_{R+SM} strategy combines two observation types that influence particle weights in different ways: reflectance via an indirect, model-coupled observation operator, and SM via a direct state observation. While DA_{R+SM} works well in the synthetic experiment, where both observation operators are fully consistent with the truth, its performance in real applications depends much on the reliability of each data source. Since SM offers temporally more continuous observations that can be assimilated regularly throughout the growing season, it has a stabilizing effect on the assimilation scheme. Reflectance observations, due to data gaps, unmodeled processes and biases, can counteract the SM stabilizing effect with their influence on particle weights. Within the resampling and perturbation process, this may lead to the selection of parameter sets that represent a compromise between conflicting constraints rather than an optimal solution. In the real-case experiment, while in 2023 the assimilation of SM corrected the inconsistencies introduced by reflectance, in 2022, its positive effect was reduced. Overall, DA_{R+SM} showed comparable results to single-source assimilations, in some cases outperforming some of them. Nevertheless, this strategy did not outperform all of the single-source assimilations, in contrast with other studies (Huang et al., 2024b; Lu et al., 2021; Pan et al., 2019). This behavior illustrates that joint assimilation can be advantageous over single-source assimilation, depending on the degree of complementarity and consistency between the assimilated observations.

A limitation of this study is represented by the mean biomass values used for validation. The high standard deviation relative to the mean clearly shows a large spatial heterogeneity across the field. Given the limited number of samples, the uncertainty associated with the measured mean biomass is rather high.

The high resolution of Sentinel-2, and the stabilizing effect of SMAP data, together with the reasonable results obtained with DA_{R+SM} on a field basis, allowed the calculation of a pixel-based biomass map. The resulting maps were evaluated in terms of biomass range and plausibility of the pattern. Spatially heterogeneous patterns of biomass distribution were clearly visible across the field in 2023. This gradient is in line with the visual observation of the field and the slight slope in the southern direction. Higher soil density and shading effects of the neighbouring forest could explain the lower biomass in the southern parts of the field. In contrast, although spatial variability was present in 2022, its magnitude was small relative to total biomass. This field does not show such a distinct gradient in geomorphology or impact of the surrounding vegetation in comparison to the 2023 field. This limited magnitude of spatial variability in the assimilated reflectance likely resulted in similar particle weights across pixels, which in turn produced weak spatial contrasts in the estimated biomass.

Conclusion

This study demonstrated the ability to assimilate Sentinel-2 reflectance and SMAP data into APSIM, both independently and simultaneously. DA was performed with a PF, in which key input model parameters were perturbed and resampled based on observational consistency. The scheme effectively linked observations, model states and parameter uncertainty, allowing the strengths and limitations of different assimilation strategies to be systematically evaluated.

The method was first tested through a synthetic experiment, which showed that the DA scheme could adequately update the model state and parameters when assimilating reflectance. Optical reflectance data are directly linked to photosynthetic activity and biomass, and their assimilation could help in capturing crop variation within a field. Moreover, the assimilation of SM data could help in reducing the ensemble spread and improving the robustness of the simulations.

Under real conditions, the assimilation of cloud-free Sentinel-2 data resulted in effective performance when more observations were available, particularly during the early stages of the growing season, and in nominal conditions, with no drought events. In comparison to the synthetic experiment, errors resulted in higher values due to the uncertainties related to the satellite sensors and the APSIM-PROSAIL coupling scheme, which were absent under ideal conditions.

The assimilation of real SM helped in stabilizing the model, filling the data gaps of Sentinel-2, and ensuring an overall increase in the accuracy of biomass estimation. Since the combined assimilation of reflectance and SM outperformed the single-source assimilation in most of the cases, it was further implemented for the generation of biomass maps. Sentinel-2 spatial resolution and SMAP temporal resolution resulted satisfactory in capturing the spatiotemporal variability of the crop maize within the fields.

While SMAP data proved effective in this assimilation scheme, it was also affected by data gaps. In the future, more advanced microwave sensors will be available. ESA's upcoming Radar Observing System for Europe in L-band (ROSE-L) mission shall be a new source of SM estimates. ROSE-L will support the existing Copernicus C-band SAR systems, ensuring to enhance near-surface SM monitoring by extending its coverage both temporally and spatially (Rostan et al., 2024). Such product could complement or substitute SMAP data, further improving the robustness and consistency of crop DA approaches.

Furthermore, new missions like Sentinel-2 Next Generation (NG) can increase the availability of data during critical phenological stages and improve the results (Berger et al., 2026). Beside multi-spectral data, hyperspectral data derived by the Hyperspectral Precursor of the Application Mission (Prisma) or the Environmental Mapping and Analysis Program (EnMAP) could be a valuable source of information (Candela et al., 2016; Chabrillat et al., 2024). However, these data are not available regularly for all regions. With the upcoming Copernicus Hyperspectral Imaging Mission for the Environment (CHIME) mission, new opportunities for integrating hyperspectral data will come up. In general, the synergistic use of data form different spectral domains can and shall be exploited further as described in Berger et al. (2026).

Acknowledgements

This work was supported by the by the TERESA SUP project (ESA Contract No. 4000145913/24/I-DT-bgh) and the ESA EXPRO project LUXSCAT (ESA Contract No. 4000138392/22/NL/SD). Furthermore, we thank EU COST (European Cooperation in Science and Technology) Action CA22136 “Pan-European Network of Green Deal Agriculture and Forestry Earth Observation Science” (PANGEOS) for support, exchange and inspiration.

Authorship contribution statement

Manuela Montella contributed to the methodology, conducted the investigation and formal analysis, prepared visualizations, wrote the original draft and was responsible for the data curation. Christian Bossung provided resources, contributed to data curation, to writing the original draft and to writing, review, and editing. Thanh Huy Nguyen provided resources, contributed to writing the original draft and to writing, review, and editing. Marco Chini contributed to writing, review, and editing. Jean François Iffly provided resources. Thomas Udelhoven contributed to writing, review, and editing. Julia Kubanek and Zoltan Szantoi supported the project and experiment, and contributed to review. Miriam Machwitz conceived the study, designed the methodology, contributed to writing the original draft, to writing, review, and editing, and provided supervision.

Conflict of Interest The authors declare that they have no conflict of interest.

Appendix

Table 6 - Climatic conditions during maize growth season in the study area.

Year	Daily solar radiation (MJ/m2)	Daily temperature (°C)	Total precipitation (mm)
2022	20.4	16.8	257
2023	18.9	16.8	307

Table 7 - LIDFa values corresponding to APSIM phenological stages.

LIDFa (°)	APSIM	
	Phenology Stage Range	Phenology Name
40°	0-4	Sowing to Emergence
50°	5-6	Floral Initiation to Flag Leaf
60°	7	Flowering
70°	8-8.9	Start Grain Fill

Table 8 - Properties of Sentinel-2 bands used in this research.

Band	Sentinel-2	
	Central wavelength [nm]	Spatial resolution [m]
B3 - Green	560	10
B4 - Red	665	10
B5 - Red edge	705	20
B6 - Red edge	740	20
B7 - Red edge	783	20
B8- NIR	842	10
B9 - Water vapour	945	60
B11 - SWIR	1610	20
B12 - SWIR	2190	20

References

Administration des services techniques de l’agriculture (ASTA). (2026). Agrimeteo Luxembourg meteorological station data. Agrimeteo. https://www.agrimeteo.lu

Baret, F., Jacquemoud, S., Guyot, G., & Leprieur, C. (1992). Modeled analysis of the biophysical nature of spectral shifts and comparison with information content of broad bands. Remote Sensing of Environment, 41(2-3), 133–142. https://doi.org/10.1016/0034-4257 (92)90073-S

Berger, K., Atzberger, C., Danner, M., D’Urso, G., Mauser, W., Vuolo, F., & Hank, T. (2018). Evaluation of the PROSAIL Model Capabilities for Future Hyperspectral Model Environments: A Review Study. Remote Sensing, 10(1), 85. https://doi.org/10.3390/rs10010085

Berger, K., Hostert, P., Schlerf, M., Immitzer, M., Szantoi, Z., Okujeni, A., Foerster, S., Colditz, R., Giardino, C., Machwitz, M., Weiss, M., Defourny, P., Kutser, T., Remeta, P., Foerster, M., Féret, J.-B., Asadzadeh, S., Chabrillat, S., Croft, H., . . . Herold, M. (2026). Advancing optical earth observation for EU policies: Needs, opportunities, recommendations. Environmental Sciences Europe. Advance online publication. https://doi.org/10.1186/s12302-026-01346-3

Brocca, L., Hasenauer, S., Lacava, T., Melone, F., Moramarco, T., Wagner, W., Dorigo, W., Matgen, P., Martínez-Fernández, J., Llorens, P., Latron, J., Martin, C., & Bittelli, M. (2011). Soil moisture estimation through ASCAT and AMSR-E sensors: An intercomparison and validation study across Europe. Remote Sensing of Environment, 115(12), 3390–3408. https://doi.org/10.1016/j.rse.2011.08.003

Brown, H. E., Huth, N. I., Holzworth, D. P., Teixeira, E. I., Zyskowski, R. F., Hargreaves, J. N., & Moot, D. J. (2014). Plant Modelling Framework: Software for building and running crop models on the APSIM platform. Environmental Modelling & Software, 62, 385–398. https://doi.org/10.1016/j.envsoft.2014.09.005

Candela, L., Formaro, R., Guarini, R., Loizzo, R., Longo, F., & Varacalli, G. (2016). The PRISMA mission. In 2016 IEEE International Geoscience and Remote Sensing Symposium (IGARSS) (pp. 253–256). IEEE. https://doi.org/10.1109/IGARSS.2016.7729057

Chabrillat, S., Foerster, S., Segl, K., Beamish, A., Brell, M., Asadzadeh, S., Milewski, R., Ward, K. J., Brosinsky, A., Koch, K., Scheffler, D., Guillaso, S., Kokhanovsky, A., Roessner, S., Guanter, L., Kaufmann, H., Pinnel, N., Carmona, E., Storch, T., . . . Fischer, S. (2024). The EnMAP spaceborne imaging spectroscopy mission: Initial scientific results two years after launch. Remote Sensing of Environment, 315, 114379. https://doi.org/10.1016/j.rse.2024.114379

Chakrabarti, S., Bongiovanni, T., Judge, J., Zotarelli, L., & Bayer, C. (2014). Assimilation of SMOS Soil Moisture for Quantifying Drought Impacts on Crop Yield in Agricultural Regions. IEEE Journal of Selected Topics in Applied Earth Observations and Remote Sensing, 7(9), 3867–3879. https://doi.org/10.1109/JSTARS.2014.2315999

Charoenhirunyingyos, S., Honda, K., Kamthonkiat, D., & Ines, A. V. M. (2011). Soil hydraulic parameters estimated from satellite information through data assimilation. International Journal of Remote Sensing, 32(23), 8033–8051. https://doi.org/10.1080/01431161.2010.532170

Copernicus Data Space Ecosystem (2023, March 30). Sentinel-2. Copernicus Data Space Ecosystem. https://dataspace.copernicus.eu/data-collections/copernicus-sentinel-data/sentinel-2

Entekhabi, D., Yueh, S., O'neill, P., Kellogg, K., Allen, A., Bindlish, R., Molly Brown, E., Chan, S., Colliander, A., Crow, W., Das, N., Lannoy, G., Dunbar, R., Edelstein, W., Entin, J., Escobar, V., Shawn Goodman, D., Jackson, T., Jai, B., . . . West, R. (2014). SMAP Handbook–Soil Moisture Active Passive: Mapping Soil Moisture and Freeze/Thaw from Space. https://www.semanticscholar.org/paper/SMAP-Handbook%E2%80%93Soil-Moisture-Active-Passive%3A-Mapping-Entekhabi-Yueh/8ba9c2e6277b1960c36192f68dd50e0041054fe8

Delécolle, R., Maas, S. J., Guérif, M., & Baret, F. (1992). Remote sensing and crop production models: present trends. ISPRS Journal of Photogrammetry and Remote Sensing, 47(2-3), 145–161. https://doi.org/10.1016/0924-2716(92)90030-D

Dorigo, W. A., Zurita-Milla, R., Wit, A. de [A.J.W.], Brazile, J., Singh, R., & Schaepman, M. E. (2007). A review on reflective remote sensing and data assimilation techniques for enhanced agroecosystem modeling. International Journal of Applied Earth Observation and Geoinformation, 9(2), 165–193. https://doi.org/10.1016/j.jag.2006.05.003

Douc, R., Cappé, O., & Moulines, E. (2005). Comparison of Resampling Schemes for Particle Filtering. Image and Signal Processing and Analysis. https://arxiv.org/pdf/cs/0507025

Dwyer, L. M., Stewart, D. W., Gregorich, E., Anderson, A. M., Ma, B. L., & Tollenaar, M. (1995). Quantifying the nonlinearity in chlorophyll meter response to corn leaf nitrogen concentration. Canadian Journal of Plant Science, 75(1), 179–182. https://doi.org/10.4141/cjps95-030

El Sharif, H., Wang, J [Jingfeng], & Georgakakos, A. P. (2015). Modeling Regional Crop Yield and Irrigation Demand Using SMAP Type of Soil Moisture Data. Journal of Hydrometeorology, 16(2), 904–916. https://doi.org/10.1175/JHM-D-14-0034.1

El-Hendawy, S. E., Alotaibi, M., Al-Suhaibani, N., Al-Gaadi, K., Hassan, W., Dewir, Y. H., Emam, M. A. E.-G., Elsayed, S., & Schmidhalter, U. (2019). Comparative Performance of Spectral Reflectance Indices and Multivariate Modeling for Assessing Agronomic Parameters in Advanced Spring Wheat Lines Under Two Contrasting Irrigation Regimes. Frontiers in Plant Science, 10, 1537. https://doi.org/10.3389/fpls.2019.01537

Esri. (2015, July 7). World Hillshade. https://services.arcgisonline.com/arcgis/rest/services/Elevation/World_Hillshade/MapServer

Europe NUTS 0 Demographics and Boundaries. (2023). Esri. https://services.arcgis.com/P3ePLMYs2RVChkJx/arcgis/rest/services/Europe_NUTS_0_Demographics_and_Boundaries/FeatureServer

Evensen, G. (2003). The Ensemble Kalman Filter: Theoretical formulation and practical implementation. Ocean Dynamics, 53(4), 343–367. https://doi.org/10.1007/s10236-003-0036-9

Ezui, K. S., Leffelaar, P. A., Franke, A. C., Mando, A., & Giller, K. E. (2018). Simulating drought impact and mitigation in cassava using the LINTUL model. Field Crops Research, 219, 256–272. https://doi.org/10.1016/J.FCR.2018.01.033

Feret, J.-B., François, C., Asner, G. P., Gitelson, A. A [Anatoly A.], Martin, R. E., Bidel, L. P., Ustin, S. L., Le Maire, G., & Jacquemoud, S [Stéphane] (2008). PROSPECT-4 and 5: Advances in the leaf optical properties model separating photosynthetic pigments. Remote Sensing of Environment, 112(6), 3030–3043. https://doi.org/10.1016/j.rse.2008.02.012

Féret, J.-B., Gitelson, A. A., Noble, S. D., & Jacquemoud, S [S.] (2017). PROSPECT-D: Towards modeling leaf optical properties through a complete lifecycle. Remote Sensing of Environment, 193, 204–215. https://doi.org/10.1016/j.rse.2017.03.004

Gavasso-Rita, Y. L., Papalexiou, S. M., Li, Y [Yanping], Elshorbagy, A., Li, Z [Zhenhua], & Schuster-Wallace, C. (2024). Crop models and their use in assessing crop production and food security: A review. Food and Energy Security, 13(1), Article e503. https://doi.org/10.1002/fes3.503

Hengl, T., Mendes de Jesus, J., Heuvelink, G. B. M., Ruiperez Gonzalez, M., Kilibarda, M., Blagotić, A., Shangguan, W., Wright, M. N., Geng, X., Bauer-Marschallinger, B., Guevara, M. A., Vargas, R., MacMillan, R. A., Batjes, N. H., Leenaars, J. G. B., Ribeiro, E., Wheeler, I., Mantel, S., & Kempen, B. (2017). Soilgrids250m: Global gridded soil information based on machine learning. PLOS ONE, 12(2), e0169748. https://doi.org/10.1371/journal.pone.0169748

Holzworth, D., Huth, N. I., Fainges, J., Brown, H., Zurcher, E., Cichota, R., Verrall, S., Herrmann, N. I., Zheng, B., & Snow, V. (2018). APSIM Next Generation: Overcoming challenges in modernising a farming systems model. Environmental Modelling & Software, 103, 43–51. https://doi.org/10.1016/j.envsoft.2018.02.002

Huang, J., Gómez-Dans, J. L., Huang, H., Ma, H [Hongyuan], Wu, Q., Lewis, P. E., Liang, S., Chen, Z., Xue, J.-H., Wu, Y., Zhao, F., Wang, J [Jing], & Xie, X. (2019a). Assimilation of remote sensing into crop growth models: Current status and perspectives. Agricultural and Forest Meteorology, 276-277, 107609. https://doi.org/10.1016/j.agrformet.2019.06.008

Huang, J., Ma, H [Hongyuan], Sedano, F., Lewis, P., Liang, S., Wu, Q., Su, W., Zhang, X., & Zhu, D. (2019b). Evaluation of regional estimates of winter wheat yield by assimilating three remotely sensed reflectance datasets into the coupled WOFOST–PROSAIL model. European Journal of Agronomy, 102, 1–13. https://doi.org/10.1016/j.eja.2018.10.008

Huang, J., Song, J., Huang, H., Zhuo, W., Niu, Q., Wu, S., Ma, H [Han], & Liang, S. (2024a). Progress and perspectives in data assimilation algorithms for remote sensing and crop growth model. Science of Remote Sensing, 10, 100146. https://doi.org/10.1016/j.srs.2024.100146

Huang, J., Tian, L., Liang, S., Ma, H [Hongyuan], Becker-Reshef, I., Huang, Y., Su, W., Zhang, X., Zhu, D., & Wu, W. (2015). Improving winter wheat yield estimation by assimilation of the leaf area index from Landsat TM and MODIS data into the WOFOST model. Agricultural and Forest Meteorology, 204, 106–121. https://doi.org/10.1016/j.agrformet.2015.02.001

Huang, X., Zhao, Y., Guo, T., & Mao, X. (2024b). Enhancing SWAP simulation accuracy via assimilation of leaf area index and soil moisture under different irrigation, film mulching and maize varieties conditions. Computers and Electronics in Agriculture, 218, 108625. https://doi.org/10.1016/j.compag.2024.108625

Ines, A. V., Das, N. N., Hansen, J. W., & Njoku, E. G [Eni G.] (2013). Assimilation of remotely sensed soil moisture and vegetation with a crop simulation model for maize yield prediction. Remote Sensing of Environment, 138, 149–164. https://doi.org/10.1016/j.rse.2013.07.018

Jackson, T., O'Neill, P., & Njoku, E., Chan, S., Bindlish, R., Colliander, A., Chen, F., Burgin M., Dunbar, S., Piepmeier, J., Cosh, M., Caldwell, T., Walker, J., Wu, X., Berg, A., Rowlandson, T., Pacheco, A., McNairn, H., Thibeault, M., Martínez-Fernández, J., González-Zamora, Á., Seyfried, M., Bosch, D., Starks, P., Goodrich, D., Prueger, J., Su, Z., van der Velde, R., Asanuma, J., Palecki, M., Small, E., Zreda, M., Calvet, J., Crow, W., Kerr, Y., Yueh, S., Entekhabi, D. (2016). Calibration and Validation for the

L2/3_ SM_P Version 3 Data Products, SMAP Project, JPL D-93720, Jet Propulsion Laboratory, Pasadena, CA.

Jacquemoud, S., Verhoef, W., Baret, F., Bacour, C., Zarco-Tejada, P. J., Asner, G. P., François, C., & Ustin, S. L. (2009). PROSPECT+SAIL models: A review of use for vegetation characterization. Remote Sensing of Environment, 113, S56-S66. https://doi.org/10.1016/j.rse.2008.01.026

Jiang, Z., Chen, Z., Chen, J., Liu, J., Ren, J., Li, Z [Zongnan], Sun, L., & Li, H. (2014). Application of Crop Model Data Assimilation With a Particle Filter for Estimating Regional Winter Wheat Yields. IEEE Journal of Selected Topics in Applied Earth Observations and Remote Sensing, 7(11), 4422–4431. https://doi.org/10.1109/JSTARS.2014.2316012

Joshi, V. R., Thorp, K. R., Coulter, J. A., Johnson, G. A., Porter, P. M., Strock, J. S., & Garcia y Garcia, A. (2019). Improving Site-Specific Maize Yield Estimation by Integrating Satellite Multispectral Data into a Crop Model. Agronomy, 9(11), 719. https://doi.org/10.3390/agronomy9110719

Kaur, R., Tiwari, R. K., Maini, R., & Singh, S. (2023). A Framework for Crop Yield Estimation and Change Detection Using Image Fusion of Microwave and Optical Satellite Dataset. Quaternary, 6(2), 28. https://doi.org/10.3390/quat6020028

Keating, B., Carberry, P., Hammer, G., Probert, M., Robertson, M [M.J], Holzworth, D., Huth, N [N.I], Hargreaves, J., Meinke, H., Hochman, Z., McLean, G., Verburg, K., Snow, V., Dimes, J., Silburn, M., Wang, E., Brown, S., Bristow, K., Asseng, S., . . . Smith, C. (2003). An overview of APSIM, a model designed for farming systems simulation. European Journal of Agronomy, 18(3-4), 267–288. https://doi.org/10.1016/S1161-0301(02)00108-9

Kerr, Y. H., Waldteufel, P., Wigneron, J.-P., Martinuzzi, J., Font, J., & Berger, M. (2001). Soil moisture retrieval from space: the Soil Moisture and Ocean Salinity (SMOS) mission. IEEE Transactions on Geoscience and Remote Sensing, 39(8), 1729–1735. https://doi.org/10.1109/36.942551

Knörzer, H., Lawes, R., Robertson, M., Graeff-Hönninger, S., & Claupein, W. (2011). Evaluation and Per formance of the APSIM Crop Growth Model for German Winter Wheat, Maize and Fieldpea Varieties in Monocropping and Intercropping Systems. Journal of Agricultural Science and Technology, 1, 698–717. https://www.researchgate.net/publication/284727955_Evaluation_and_Performance_of_the_APSIM_Crop_Growth_Model_for_German_Winter_Wheat_Maize_and_Fieldpea_Varieties_in_Monocropping_and_Intercropping_Systems

Kuusk, A. (2001). A two-layer canopy reflectance model. Journal of Quantitative Spectroscopy and Radiative Transfer, 71(1), 1–9. https://doi.org/10.1016/S0022-4073(01)00007-3

Li, W., Wang, Y [Yunpeng], Yang, J., & Deng, Y. (2022). Time-Lag Effect of Vegetation Response to Volumetric Soil Water Content: A Case Study of Guangdong Province, Southern China. Remote Sensing, 14(6), 1301. https://doi.org/10.3390/rs14061301

Li, Y [Yan], Zhou, Q., Zhou, J., Zhang, G., Chen, C., & Wang, J [Jing] (2014). Assimilating remote sensing information into a coupled hydrology-crop growth model to estimate regional maize yield in arid regions. Ecological Modelling, 291, 15–27. https://doi.org/10.1016/j.ecolmodel.2014.07.013

Li, Y [Yanyan], Yao, Y., Du, M., Dong, L., Yuan, J., & Li, G. (2025). APSIM NG Model Simulation of Soil N2O Emission from the Dry-Crop Wheat Field and Its Parameter Sensitivity Analysis. Agronomy, 15(4), 834. https://doi.org/10.3390/agronomy15040834

Liu, Z., Xu, Z., Bi, R., Wang, C., He, P., Jing, Y., & Yang, W. (2021). Estimation of Winter Wheat Yield in Arid and Semiarid Regions Based on Assimilated Multi-Source Sentinel Data and the CERES-Wheat Model. Sensors (Basel, Switzerland), 21(4). https://doi.org/10.3390/s21041247

Lobos, G. A., Escobar-Opazo, A., Estrada, F., Romero-Bravo, S., Garriga, M., Del Pozo, A., Poblete-Echeverría, C., Gonzalez-Talice, J., González-Martinez, L., & Caligari, P. (2019). Spectral Reflectance Modeling by Wavelength Selection: Studying the Scope for Blueberry Physiological Breeding under Contrasting Water Supply and Heat Conditions. Remote Sensing, 11(3), 329. https://doi.org/10.3390/rs11030329

Lu, Y., Chibarabada, T. P., Ziliani, M. G., Onema, J.-M. K., McCabe, M. F., & Sheffield, J. (2021). Assimilation of soil moisture and canopy cover data improves maize simulation using an under-calibrated crop model. Agricultural Water Management, 252, 106884. https://doi.org/10.1016/j.agwat.2021.106884

Luo, L., Sun, S., Xue, J., Gao, Z., Zhao, J., Yin, Y., Gao, F., & Luan, X. (2023). Crop yield estimation based on assimilation of crop models and remote sensing data: A systematic evaluation. Agricultural Systems, 210, 103711. https://doi.org/10.1016/j.agsy.2023.103711

Luxembourg Canton Boundaries. (2025). Esri. https://services.arcgis.com/P3ePLMYs2RVChkJx/arcgis/rest/services/LUX_Boundaries_view/FeatureServer

Ma, C., Liu, M., Ding, F., Li, C., Cui, Y., Chen, W., & Wang, Y [Yilin] (2022). Wheat growth monitoring and yield estimation based on remote sensing data assimilation into the SAFY crop growth model. Scientific Reports, 12(1), 5473. https://doi.org/10.1038/s41598-022-09535-9

Machwitz, M., Giustarini, L., Bossung, C., Frantz, D., Schlerf, M., Lilienthal, H., Wandera, L., Matgen, P [Patrick], Hoffmann, L [Lucien], & Udelhoven, T. (2014). Enhanced biomass prediction by assimilating satellite data into a crop growth model. Environmental Modelling & Software, 62, 437–453. https://doi.org/10.1016/j.envsoft.2014.08.010

Marin, F., Jones, J. W., & Boote, K. J. (2017). A Stochastic Method for Crop Models: Including Uncertainty in a Sugarcane Model. Agronomy Journal, 109(2), 483–495. https://doi.org/10.2134/agronj2016.02.0103

Markwell, J., Osterman, J. C., & Mitchell, J. L. (1995). Calibration of the Minolta SPAD-502 leaf chlorophyll meter. Photosynthesis Research, 46(3), 467–472. https://doi.org/10.1007/BF00032301

Matgen, P., Montanari, M., Hostache, R., Pfister, L., Hoffmann, L., Plaza, D., Pauwels, V. R. N., Lannoy, G. J. M. de, Keyser, R. de, & Savenije, H. H. G. (2010). Towards the sequential assimilation of SAR-derived water stages into hydraulic models using the Particle Filter: proof of concept. Hydrology and Earth Sys tem Sciences, 14(9), 1773–1785. https://doi.org/10.5194/hess-14-1773-2010

Ministère de l'Agriculture, de l'Alimentation et de la Viticulture. (2023). Rapport Annuel 2023. https://agriculture.public.lu/de/veroeffentlichungen/agrarpolitik/rapport-annuel/2023.html

Mishra, A., Vu, T., Veettil, A. V., & Entekhabi, D. (2017). Drought monitoring with soil moisture active passive (SMAP) measurements. Journal of Hydrology, 552, 620–632. https://doi.org/10.1016/j.jhydrol.2017.07.033

Moradkhani, H., Hsu, K.-L., Gupta, H., & Sorooshian, S. (2005). Uncertainty assessment of hydrologic model states and parameters: Sequential data assimilation using the particle filter. Water Resources Research, 41(5), Article 2004WR003604. https://doi.org/10.1029/2004WR003604

Njoku, E. G., Jackson, T. J., Lakshmi, V., Chan, T. K., & Nghiem, S. V. (2003). Soil moisture retrieval from AMSR-E. IEEE Transactions on Geoscience and Remote Sensing, 41(2), 215–229. https://doi.org/10.1109/tgrs.2002.808243

Orlova, Y., & Linker, R. (2023). Data assimilation with sensitivity-based particle filter: A simulation study with AquaCrop. Computers and Electronics in Agriculture, 204, 107538. https://doi.org/10.1016/j.compag.2022.107538

Owe, M., Jeu, R. de, & Holmes, T. (2008). Multisensor historical climatology of satellite-derived global land surface moisture. Journal of Geophysical Research: Earth Surface, 113(F1), Article 2007JF000769. https://doi.org/10.1029/2007JF000769

Owe, M., & van de Griend, A. A. (1998). Comparison of soil moisture penetration depths for several bare soils at two microwave frequencies and implications for remote sensing. Water Resources Research, 34(9), 2319–2327. https://doi.org/10.1029/98WR01469

Pan, H., Chen, Z., Allard, d. W., & Ren, J. (2019). Joint Assimilation of Leaf Area Index and Soil Moisture from Sentinel-1 and Sentinel-2 Data into the WOFOST Model for Winter Wheat Yield Estimation. Sensors (Basel, Switzerland), 19(14). https://doi.org/10.3390/s19143161

Passioura, J. B. (1996). Simulation Models: Science, Snake Oil, Education, or Engineering? Agronomy Journal, 88(5), 690–694. https://doi.org/10.2134/agronj1996.00021962008800050002x

Reichle, R. H., & Koster, R. D. (2004). Bias reduction in short records of satellite soil moisture. Geophysical Research Letters, 31(19), Article 2004GL020938. https://doi.org/10.1029/2004GL020938

Reichle, R. H. (2008). Data assimilation methods in the Earth sciences. Advances in Water Resources, 31(11), 1411–1418. https://doi.org/10.1016/j.advwatres.2008.01.001

Rostan, F., Mak, K., Alberti, M. von, Bauleo, A., & Gebert, N. (2024). Rose-L SAR Instrument Development Status and Mission Performance Prediction. In IGARSS 2024 - 2024 IEEE International Geoscience and Remote Sensing Symposium (pp. 6618–6620). IEEE. https://doi.org/10.1109/IGARSS53475.2024.10642943

Salamon, P., & Feyen, L. (2009). Assessing parameter, precipitation, and predictive uncertainty in a distributed hydrological model using sequential data assimilation with the particle filter. Journal of Hydrology, 376(3-4), 428–442. https://doi.org/10.1016/j.jhydrol.2009.07.051

Schley, L., Dufrêne, M., Krier, A., & Frantz, A. C. (2008). Patterns of crop damage by wild boar (Sus scrofa)in Luxembourg over a 10-year period. European Journal of Wildlife Research, 54(4), 589–599. https://doi.org/10.1007/s10344-008-0183-x

The State of Food Security and Nutrition in the World 2025. (2025). FAO; IFAD; UNICEF; WFP; WHO. https://doi.org/10.4060/cd6008en

Steduto, P., Hsiao, T. C., Raes, D., & Fereres, E. (2009). AquaCrop—The FAO Crop Model to Simulate Yield Response to Water: I. Concepts and Underlying Principles. Agronomy Journal, 101(3), 426–437. https://doi.org/10.2134/AGRONJ2008.0139S

Stevens, A., Udelhoven, T., Denis, A., Tychon, B., Lioy, R., Hoffmann, L [Lucien], & van Wesemael, B. (2010). Measuring soil organic carbon in croplands at regional scale using airborne imaging spectroscopy. Geoderma, 158(1-2), 32–45. https://doi.org/10.1016/j.geoderma.2009.11.032

Su, W., Huang, J., Liu, D., & Zhang, M. (2019). Retrieving Corn Canopy Leaf Area Index from Multitemporal Landsat Imagery and Terrestrial LiDAR Data. Remote Sensing, 11(5), 572. https://doi. org/10. 3390/rs11 050572

van Dam, J. C., Groenendijk, P., Hendriks, R. F., & Kroes, J. G. (2008). Advances of Modeling Water Flow in Variably Saturated Soils with SWAP. Vadose Zone Journal, 7(2), 640–653. https://doi. org/10. 2136/vzj 2007.0060

van der Schalie, R., van der Vliet, M., Rodríguez-Fernández, N., Dorigo, W [Wouter], Scanlon, T., Preimesberge r, W., Madelon, R., & Jeu, R. de (2021). L-Band Soil Moisture Retrievals Using Microwave Based Temperature and Filtering. Towards Model-Independent Climate Data Records. Remote Sensing, 13(13), 2480. https://doi.org/10.3390/rs13132480

van der Tol, C., Verhoef, W., Timmermans, J., Verhoef, A., & Su, Z. (2009). An integrated model of soil-canopy spectral radiances, photosynthesis, fluorescence, temperature and energy balance. Biogeosciences, 6(12), 3109–3129. https://doi.org/10.5194/bg-6-3109-2009

van Diepen, C. A., Wolf, J., van Keulen, H., & Rappoldt, C. (1989). Wofost: A simulation model of crop production. Soil Use and Management, 5(1), 16–24. https://doi.org/10.1111/j.1475-2743.1989.tb00755.x

Verhoef, W. (1984). Light scattering by leaf layers with application to canopy reflectance modeling: The SAIL model. Remote Sensing of Environment, 16(2), 125–141. https://doi.org/10.1016/0034-4257(84)90057-9

Wagner, M. P., Slawig, T., Taravat, A., & Oppelt, N. (2020). Remote Sensing Data Assimilation in Dynamic Crop Models Using Particle Swarm Optimization. ISPRS International Journal of Geo-Information, 9(2), 105. https://doi.org/10.3390/ijgi9020105

Wang, J [Jun], Wang, Y [Yanlong], & Qi, Z. (2024). Remote Sensing Data Assimilation in Crop Growth Modeling from an Agricultural Perspective: New Insights on Challenges and Prospects. Agronomy, 14(9), 1920. https://doi.org/10.3390/agronomy14091920

Weinman, A., Linker, R., & Rozenstein, O. (2025a). Investigation of coupling DSSAT with SCOPE-RTMo via sensitivity analysis and use of this coupled crop-radiative transfer model for sensitivity-based data assimilation. European Journal of Agronomy, 162, 127431. https://doi.org/10.1016/j.eja.2024.127431

Weinman, A., Linker, R., & Rozenstein, O. (2025b). Uncertainty propagation analysis of remote sensing data in a coupled crop-radiative transfer model using particle filter and winding stairs. Environmental Modelling & Software, 193, 106645. https://doi.org/10.1016/j.envsoft.2025.106645

Weinman, A., Malachy, N., Linker, R., & Rozenstein, O. (2025c). Assimilation of UAV multispectral imagery into a coupled DSSAT-CROPGRO − SCOPE model for processing tomatoes. Computers and Electronics in Agriculture, 236, 110460. https://doi.org/10.1016/j.compag.2025.110460

Williams, J. R., Jones, C. A., Kiniry, J. R., & Spanel, D. A. (1989). The EPIC Crop Growth Model. Transactions of the ASAE, 32(2), 497–511. https://doi.org/10.13031/2013.31032

World Imagery. (2009). Esri. https://services.arcgisonline.com/ArcGIS/rest/services/World_Imagery/MapServer

Xie, Y., Wang, P., Sun, H., Zhang, S., & Li, L. (2017). Assimilation of Leaf Area Index and Surface Soil Moisture With the CERES-Wheat Model for Winter Wheat Yield Estimation Using a Particle Filter Algorithm. IEEE Journal of Selected Topics in Applied Earth Observations and Remote Sensing, 10(4), 1303–1316. https://doi.org/10.1109/JSTARS.2016.2628809

Yokoyama, Y., Wit, A. de [Allard], Matsui, T., & Tanaka, T. S. T. (2024). Accuracy and robustness of a plant-level cabbage yield prediction system generated by assimilating UAV-based remote sensing data into a crop simulation model. Precision Agriculture, 25(6), 2685–2702. https://doi.org/10.1007/s11119-024-10192-3

Zhang, L., Guo, C. L., Zhao, L. Y., Zhu, Y., Cao, W. X., Tian, Y. C., Cheng, T., & Wang, X. (2016). Estimating wheat yield by integrating the WheatGrow and PROSAIL models. Field Crops Research, 192, 55–66. https://doi.org/10.1016/j.fcr.2016.04.014

Zhang, Y., Walker, J. P., Pauwels, V. R. N [Valentijn R. N.], & Sadeh, Y. (2022). Assimilation of Wheat and Soil States into the APSIM-Wheat Crop Model: A Case Study. Remote Sensing, 14(1), 65. https://doi.org/10.3390/rs14010065

Zhang, Z., Li, Z [Ziyue], Chen, Y., Zhang, L [Lingyan], & Tao, F. (2020). Improving regional wheat yields estimations by multi-step-assimilating of a crop model with multi-source data. Agricultural and Forest Meteorology, 290, 107993. https://doi.org/10.1016/j.agrformet.2020.107993

Zhao, H., Montzka, C., Keller, J., Li, F., Vereecken, H., & Hendricks Franssen, H.-J. (2025). How Does Assimilating SMAP Soil Moisture Improve Characterization of the Terrestrial Water Cycle in an Integrated Land Surface-Subsurface Model? Water Resources Research, 61(6), Article e2024WR038647, e2024WR038647. https://doi.org/10.1029/2024WR038647

Zheng, D., Wang, X [Xin], van der Velde, R., Ferrazzoli, P., Wen, J., Wang, Z., Schwank, M., Colliander, A., Bindlish, R., & Su, Z [Zhongbo] (2018). Impact of surface roughness, vegetation opacity and soil permittivity on L-band microwave emission and soil moisture retrieval in the third pole environment. Remote Sensing of Environment, 209, 633–647. https://doi.org/10.1016/j.rse.2018.03.011

Zhuo, W., Huang, J., Li, L., Zhang, X., Ma, H [Hongyuan], Gao, X., Huang, H., Xu, B., & Xiao, X. (2019). Assimilating Soil Moisture Retrieved from Sentinel-1 and Sentinel-2 Data into WOFOST Model to Improve Winter Wheat Yield Estimation. Remote Sensing, 11(13), 1618. https://doi.org/10.3390/rs1113 1618

Ziliani, M. G., Altaf, M. U., Aragon, B., Houborg, R., Franz, T. E., Lu, Y., Sheffield, J., Hoteit, I., & McCabe, M. F. (2022). Early season prediction of within-field crop yield variability by assimilating CubeSat data into a crop model. Agricultural and Forest Meteorology, 313, 108736. https://doi.org/10. 1016/j.agrformet.2021.108736